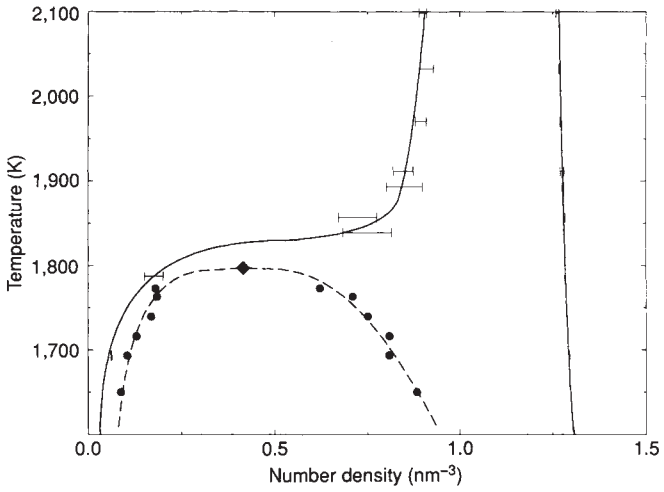

FIG. 2 Computed temperature–density phase diagram of C_{60} for temperatures in the region of 1,800 K. The solid lines are the solid–fluid coexistence lines. They were obtained by a fit to the data points (indicated by error bars) derived from free-energy calculations[7,8] at 3,218, 1,893, 1,839, 1,788 and 1,694 K and 'Clausius–Clapeyron' integration[9] between 3,218 and 1,893 K. The area between the two solid lines is a two-phase region where solid coexists with fluid. The dashed line denotes the (metastable) liquid–vapour coexistence line. It was obtained by a fit to the data points (solid circles) that were computed using the Gibbs-ensemble simulation technique of ref. 5. The solid diamond indicates the estimated location of the critical point. The fact that the critical point is located below the solid–fluid coexistence line implies that C_{60} has no liquid phase.

by integrating the Clausius–Clapeyron equation, following the scheme developed by Kofke[9].

Figure 2 shows our prediction for the phase diagram of C_{60}. The sublimation line passes 35 ± 10 K above the liquid–vapour critical point. All phases that occur below the sublimation line in Fig. 2 have a higher Gibbs free energy than the coexisting solid and vapour phases. It may be possible to reach the liquid–vapour coexistence curve by supercooling the fluid below the sublimation line. But the liquid phase that would then form is necessarily less stable than the coexisting solid and vapour phases. Our results therefore suggest that C_{60} has no stable liquid phase. To our knowledge, this would be the first example of a pure substance that has no triple point. Of course, these findings assume that the interaction potential for C_{60} proposed in ref. 1 is accurate. An improved description of the intermolecular interactions would presumably result in small shifts of the predicted phase boundaries, but this will do little to change the highly anomalous appearance of the C_{60} phase diagram. Specifically, we expect the (metastable) critical point to remain very close to the sublimation line. This has interesting consequences for the formation of solid C_{60} from the vapour phase. If C_{60} is cooled below the sublimation line, it will probably not nucleate crystals from the vapour phase because, as soon as it is cooled below the liquid–vapour spinodal (that is, the line where the homogeneous fluid becomes absolutely unstable), metastable liquid-like aggregates will form. One might think that the formation of these aggregates would assist subsequent crystallization. However, experiments[10] and simulations[11] on colloids with short-ranged attractions indicate that such aggregates do not crystallize but gelate to form rather open fractal structures. By analogy, we expect that solid C_{60} that is formed by homogeneous nucleation from the vapour phase will form an amorphous, rather than a crystalline phase. This may explain why the high-temperature synthesis of C_{60} in the gas phase often results in sooty deposits.

After we had completed this work, A. Cheng *et al.*[12] reported a similar simulation study of C_{60} in which the phase boundaries were located using a series of approximations. As a result of these approximations, a narrow liquid range was seen above 1,800 K. □

Received 7 July; accepted 19 August 1993.

1. Girifalco, L. A. *J. phys. Chem.* **96,** 858–861 (1992).
2. Pusey, P. N. in *Liquids, Freezing and Glass Transition* (eds Hansen, J. P., Levesque, D. & Zinn-Justin J.) 763–942 (North-Holland, Amsterdam, 1991).
3. Heiney, P. A. *et al. Phys. Rev. Lett.* **66,** 2911–2914 (1991).
4. Nunez-Regueiro, M. *Mod. Phys. Lett.* **B19,** 1153–1158 (1992).
5. Panagiotopoulos, A. Z. *Molec. Phys.* **61,** 813–826 (1987).
6. Smit, B., de Smedt, Ph. & Frenkel, D. *Molec. Phys.* **68,** 931–950 (1989).
7. Frenkel, D. & Ladd, A. J. C. *J. chem. Phys.* **81,** 3188–3193 (1984).
8. Meijer, E. J., Frenkel, D., LeSar, R. A. & Ladd, A. J. C. *J. chem. Phys.* **92,** 7570–7575 (1990).
9. Kofke, D. A. *J. chem. Phys.* **98,** 4149–4162 (1993).
10. Rouw, P. W. & de Kruif, C. G. *Phys. Rev.* A**39,** 5399–5408 (1989).
11. Kranendonk, W. G. T. & Frenkel, D. *Molec. Phys.* **64,** 403–424 (1988).
12. Cheng, A., Klein, M. L. & Caccamo, C. *Phys. Rev. Lett.* **71,** 1200–1203 (1993).

ACKNOWLEDGEMENTS. The work of the FOM Institute is supported by the Nederlandse Organisatie voor Wetenschappelijk Onderzoek (NWO). We acknowledge comments by M. L. Klein.

Enhanced reactivity of fullerene cations containing adjacent pentagons

Simon Petrie & Diethard K. Bohme

Department of Chemistry and Centre for Research in Earth and Space Science, York University, North York, Ontario, Canada M3J 1P3

GEOMETRICAL constraints, first identified by Euler, dictate that all of the closed carbon cages known as fullerenes must contain twelve pentagonal rings of carbon atoms[1]. In all of the fullerenes synthesized so far, each pentagon is surrounded by hexagonal rings[2]. Indeed, this has been proposed as a criterion for fullerene stability—the 'isolated-pentagon rule'[1,3]—on the basis that adjacent pentagons are expected to be chemically reactive. Buckminsterfullerene (C_{60}) is the smallest fullerene for which the isolated-pentagon rule can be satisfied; smaller, adjacent-pentagon fullerenes have not been formed in bulk, but have been identified previously as cations[4–6]. Here we report experimental evidence for the heightened chemical reactivity of cations of the adjacent-pentagon fullerenes C_{56} and C_{58}, relative to C_{60}^{x+}, which provides support for the basic assumptions underlying the isolated-pentagon rule. Our findings suggest that, if fullerenes such as C_{56} and C_{58} are produced as intermediates or byproducts of C_{60} generation either in the laboratory or in natural environments, they should form derivatives readily.

Using a selected-ion flow tube (SIFT) described elsewhere[7,8], we have observed many examples of addition reactions

$$C_{60}^{x+} + AB \rightarrow C_{60}.AB^{x+} \qquad (1)$$

for the ions C_{60}^{+}, C_{60}^{2+} and C_{60}^{3+}, and have determined that several factors influence the efficiency of reaction (1) for different charge states (x) and for different reactants (AB)[9,10]. The ions C_{60}^{x+} are generated by the impact of electrons upon vaporized C_{60}, a technique which also produces ions C_n^{x+} ($n < 60$) by the dissociative ionization of buckminsterfullerene. The molecules chosen for reaction with these latter ions were several (CH_3CN, NH_3, C_2H_4, n-C_4H_{10}) which showed little reactivity with C_{60}^{x+}, because such reactions provide scope for observable rate enhancement.

The increased reactivity of C_{56}^{x+} and C_{58}^{x+}, compared to that of C_{60}^{x+}, can be readily seen from the kinetic measurements reported in Table 1 and illustrated in Figs 1 and 2. There is a considerable amount of experimental evidence to support the assumption that C_{56}^{x+} and C_{58}^{x+} are fullerene ions. For example, collisions of

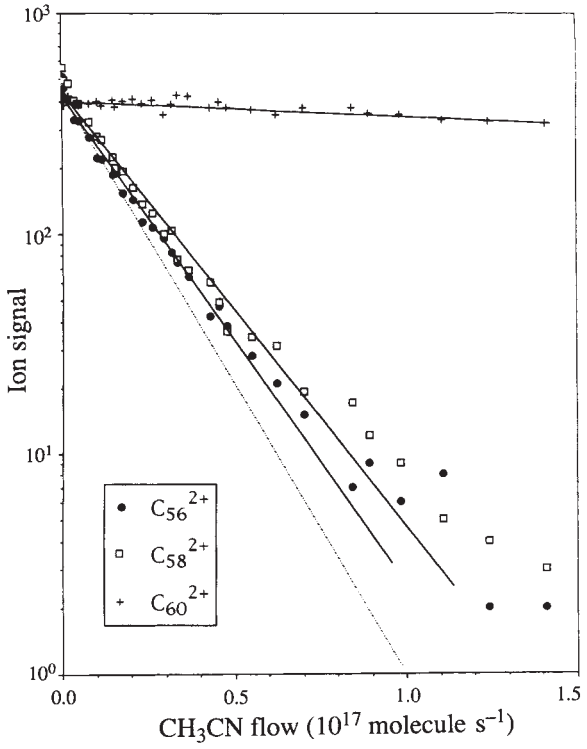

FIG. 1 Experimental data for the association reactions of C_{56}^{2+}, C_{58}^{2+} and C_{60}^{2+} with methyl cyanide, CH_3CN, performed at 294 ± 2 K and at a helium buffer gas pressure of 0.344 ± 0.001 torr. The exponential decay curves for C_{56}^{2+} and C_{58}^{2+} (which appear linear as the vertical-axis scale is logarithmic) are very much steeper than that observed for C_{60}^{2+}, indicating that the adjacent-pentagon fullerene ions C_{56}^{2+} and C_{58}^{2+} are much more reactive with CH_3CN than is C_{60}^{2+}. Rate coefficients for each ion are obtained from the least-squares line fitted to each ion signal plotted on such a graph. The corresponding ADO collision-rate coefficient is represented by the dotted line: clearly, C_{56}^{2+} and C_{58}^{2+} react with CH_3CN upon virtually every collision.

high-energy C_{60}^{x+} ($x = 1$–3) and C_{58}^{+} with helium result in formation of endohedral He adducts of the 'descendant' ions C_{60-2n}^{x+} and C_{58-2n}^{+}, respectively: the incarceration of helium within the cavities of these descendant ions indicates that the surfaces have 'healed' rapidly to retain the fullerene structure[11,12]. Further evidence is seen in the dissociation pattern for large carbon-cluster ions[13]—all even-carbon clusters larger than C_{32} lose only even numbers of carbon atoms on laser-induced fragmentation, whereas odd-carbon clusters in this size range lose an odd number of carbons. This is explained most readily by the dissociative model[13,14] which presumes that the even-carbon cluster products containing $\geqslant 32$ carbons are fully closed structures. In our own experiments, while we are able to generate substantial quantities of ions such as C_{50}^{x+}, C_{52}^{x+}, C_{54}^{x+}, C_{56}^{x+} and C_{58}^{x+} by dissociative ionization of C_{60}, we cannot produce detectable quantities of the neighbouring odd-carbon ions. This strongly suggests that the C_{60-2n}^{x+} fragment ions in our experiments are also fullerenes, and, by necessity, adjacent-pentagon fullerenes as they contain fewer than 60 atoms[1].

Of the four neutral reactants included in the present study, three react by association. The heightened efficiency of these reactions for the smaller fullerene ions C_{56}^{x+} and C_{58}^{x+} is especially significant because theory[15] predicts that, in the absence of other factors, association efficiency should decrease with the decreasing size of the reactant ion or neutral; furthermore, this effect should be small for the reactions of such large ions with small neutrals. A rationale for the enhanced reactivity of C_{56}^{x+} and C_{58}^{x+} lies in the greater sp^3 character of carbons lying at the shared edge of adjacent pentagons, as shown in Fig. 3. The sp^3 character of the carbons within the reactant fullerene ion is important because each atom in a fullerene is already bonded to three others: formation of an additional bond between a fullerene carbon atom and an atom within a neutral reactant molecule requires tetrahedral coordination about this carbon atom, and this will be easier if this atom already possesses a degree of sp^3 character. All the carbon atoms in C_{60}, and in all higher isolated-pentagon fullerenes, possess largely sp^2 character: the increasing stability of fullerenes with increasing fullerene size[16] is ascribed to the smoother, more graphite-like surface of the higher fullerenes. Inducing tetrahedral coordination at one carbon atom on

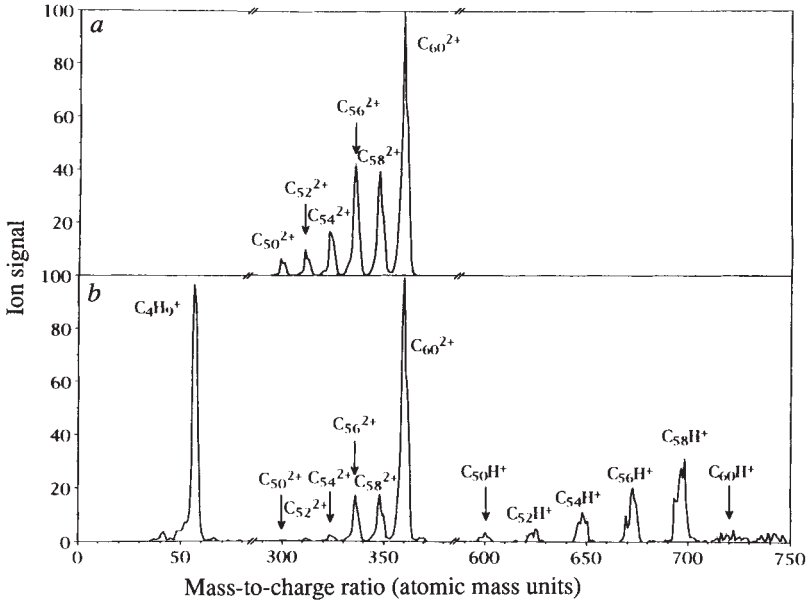

FIG. 2 Mass spectra obtained for a series of fullerene dications C_{50}^{2+}–C_{60}^{2+}, before (*a*) and after (*b*) addition of butane, C_4H_{10}, to the reaction vessel. The reaction observed for each dication is a hydride abstraction process:

$$C_n^{2+} + C_4H_{10} \rightarrow C_nH^+ + C_4H_9^+$$
$$(n = 50, 52, 54, 56, 58, 60)$$

The low reactivity of C_{60}^{2+}, in comparison to the other reactant ions, is apparent: under these conditions, C_{60}^{2+} (which is the most abundant reactant ion) produces less product ($C_{60}H^+$) than do all of the lower-mass, adjacent-pentagon fullerene dications.

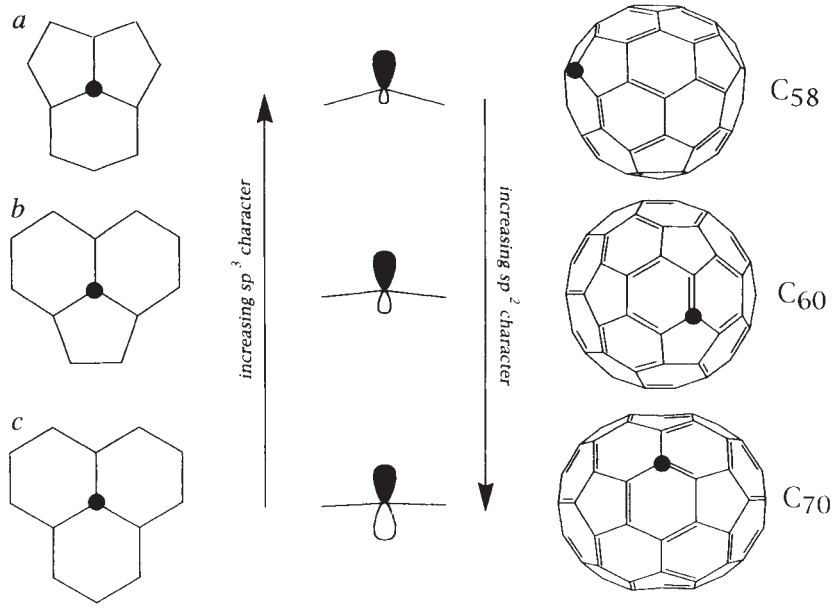

FIG. 3 An illustration of different environments for carbon atoms within fullerenes. Each carbon atom on the surface of a fullerene is involved in three pentagonal or hexagonal rings. Fullerenes smaller than C_{60} invariably possess structural features of type (*a*), involving two pentagons and one hexagon. These three rings are far from coplanar (as shown in the bond-and-orbital diagram beside (*a*)) and the orbitals of the central carbon atom are therefore expected to possess substantial sp^3 character. Structural features of type (*b*), the *only* feature found on the surface of C_{60}, involve two hexagons and one pentagon which are more nearly coplanar: the carbon atom involved here has bonds with a lower degree of sp^3 character. Fullerenes larger than C_{60} contain sites of type (*b*) but also possess structural features of type (*c*), which is also found in graphite and which has the lowest deviation from coplanarity of the three features discussed here. So, the bonding involved in this feature is expected to have a high degree of sp^2 character with little sp^3 character. The formation of a fourth chemical bond to a carbon atom, in a tetrahedral coordination, implies sp^3 hybridization at the carbon concerned in the resulting product. This process is expected to be easiest at sites which already feature a high degree of sp^3 character.

a surface such as that of C_{60}, which is constrained to remain as smooth as possible in order to maximize π overlap across the surface, is likely to be an energy-demanding process, and will only be feasible if the energy gain by means of bond formation is greater than the energy required to distort the carbon surface.

Although theoretical calculations have not, to our knowledge, predicted increased chemical reactivity for adjacent-pentagon fullerenes, they have indicated that such structures are substantially lower in thermodynamic stability than isolated-pentagon fullerenes. MNDO (modified neglect of diatomic overlap) calculations[16] suggest a destabilization energy, per pair of adjacent pentagons, of about 7 kcal mol^{-1}, which is similar to the calculated resonance destabilization for the adjacent-pentagon conjugated hydrocarbon molecule pentalene. Calculations on C_{60} isomerism[17] have indicated that a C_{60} structure with two pairs of adjacent pentagons is ~35 kcal mol^{-1} higher in energy than the global minimum buckminsterfullerene structure.

A recent experimental study of high-energy collisions of the adjacent-pentagon fullerenes C_{58}^+ and C_{68}^+ with helium has demonstrated that, in contrast to similar experiments with C_{60}^+ and C_{70}^+, the parent helium adduct is not formed in detectable quantities, although 'descendant' adducts (involving loss of C_2 units) are observed in all cases[11,12]. The failure of the adjacent-pentagon adducts to remain intact has been attributed to the relative destabilization caused by the adjacent-pentagon structural feature[12].

Our results may have implications for chemical reactions of fullerenes in interstellar clouds and circumstellar shells. It has been suggested that fullerenes may be formed in the envelopes surrounding giant carbon-rich stars[18,19] especially those with very low abundances of hydrogen. We have identified viable pathways to singly and doubly ionized fullerenes from neutral fullerenes under such conditions[20], indicating that ion-molecule reactions of these molecules may be significant in interstellar and circumstellar environments[21,22]. Growth mechanisms for fullerenes are still a subject of debate: most proposed mechanisms involve the production of fullerenes from smaller neutral or ionized carbon fragments, although a recent study suggests that rearrangement and fragmentation of larger mono-, bi- and tricyclic carbon rings can also produce fullerenes[23]. It seems possible that production of C_{60} involves the earlier, or simultaneous, formation of smaller fullerenes such as C_{58} and C_{56}. If this is the case, these smaller fullerenes will also be intermediates in, or byproducts of, the circumstellar generation of C_{60}. Our results suggest that those clusters which possess adjacent pentagons are likely to form derivatives readily in interstellar and circumstellar environments, which are expected to have spectral features distinct from those of the less-reactive fullerenes typified by C_{60}. □

TABLE 1 Reactions of C_n^{x+} ($x = 56, 58, 60$) with various compounds

Reaction	Products	k_{obs}*	k_c†	k/k_{60}‡
$C_{56}^{2+} + CH_3CN$	$C_{56} \cdot CH_3CN^{2+}$	4.3	4.96	53.8
$C_{58}^{2+} + CH_3CN$	$C_{58} \cdot CH_3CN^{2+}$	4.2	4.94	52.5
$C_{60}^{2+} + CH_3CN$	$C_{60} \cdot CH_3CN^{2+}$	0.08§	4.93	1.0
$C_{56}^{+} + NH_3$	$C_{56} \cdot NH_3^{+}$	0.0096	1.65	>9.6
$C_{58}^{+} + NH_3$	$C_{58} \cdot NH_3^{+}$	0.034	1.65	>34.0
$C_{60}^{+} + NH_3$	$C_{60} \cdot NH_3^{+}$	<0.001‖	1.65	1.0
$C_{56}^{2+} + C_2H_4$	$C_{56} \cdot C_2H_4^{2+}$	0.021	1.86	>21.0
$C_{58}^{2+} + C_2H_4$	$C_{58} \cdot C_2H_4^{2+}$	0.019	1.86	>19.0
$C_{60}^{2+} + C_2H_4$	$C_{60} \cdot C_2H_4^{2+}$	<0.001¶	1.86	1.0
$C_{56}^{2+} + n\text{-}C_4H_{10}$	$C_{56}H^+ + C_4H_9^+$	0.027	1.87	>27.0
$C_{58}^{2+} + n\text{-}C_4H_{10}$	$C_{58}H^+ + C_4H_9^+$	0.034	1.86	>34.0
$C_{60}^{2+} + n\text{-}C_4H_{10}$	$C_{60}H^+ + C_4H_9^+$	<0.001¶	1.86	1.0

* Observed effective bimolecular reaction rate coefficient (in units of 10^{-9} cm^3 molecule^{-1} s^{-1}) at 294 ± 2 K and 0.35 ± 0.01 torr of helium.

† Calculated ADO (Average-Dipole Orientation) collision rate coefficient (in units of 10^{-9} cm^3 molecule^{-1} s^{-1}) at 294 K, determined using the method of Su and Bowers[24].

‡ Rate enhancement observed for reaction, expressed as the ratio $k_{obs}(C_n^{x+}) : k_{obs}(C_{60}^{x+})$.

§ The reaction of C_{60}^{2+} was previously reported in ref. 10.

‖ The reaction of C_{60}^{+} was previously reported in ref. 25.

¶ The reaction of C_{60}^{2+} was previously reported in ref. 9.

Received 12 April; accepted 3 August 1993.

1. Kroto, H. W. *Nature* **329,** 529–531 (1987).
2. Diederich, F. & Whetten, R. L. *Accts. Chem. Res.* **25,** 119–126 (1992).
3. Smalley, R. E. *Accts. Chem. Res.* **25,** 98–105 (1992).
4. Rohlfing, E. A., Cox, D. M. & Kaldor, A. *J. chem. Phys.* **81,** 3322–3330 (1984).
5. Kroto, H. W., Heath, J. R., O'Brien, S. C., Curl, R. F. & Smalley, R. E. *Nature* **318,** 162–163 (1985).
6. von Helden, G., Hsu, M.-T., Kemper, P. R. & Bowers, M. T. *J. chem. Phys.* **95,** 3835–3837 (1991).

7. Mackay, G. I., Vlachos, G. D., Bohme, D. K. & Schiff, H. I. *Int. J. Mass Spectrom. Ion Phys.* **36,** 259–270 (1980).
8. Raksit, A. B. & Bohme, D. K. *Int. J. Mass Spectrom. Ion Phys.* **55,** 69–82 (1983).
9. Petrie, S., Javahery, G., Wang, J. & Bohme, D. K. *J. Am. chem. Soc.* **114,** 9177–9181 (1992).
10. Petrie, S., Javahery, G. & Bohme, D. K. *J. Am. chem. Soc.* **115,** 1445–1450 (1993).
11. Schwarz, H., Weiske, T., Bohme, D. K. & Hrušák, J. in *Buckminsterfullerenes* (eds Billups, W. E. & Ciufolini, M. A.) 257–283 (VCH, New York, 1993).
12. Callahan, J. H., Ross, M. M., Weiske, T. & Schwarz, H. *J. phys. Chem.* **97,** 20–22 (1993).
13. O'Brien, S. C., Heath, J. R., Curl, R. F. & Smalley, R. E. *J. chem. Phys.* **88,** 220–230 (1988).
14. Stone, A. J. & Wales, D. J. *Chem. Phys. Lett.* **128,** 501–503 (1986).
15. Herbst, E. & Dunbar, R. C. *Mon. Not. R. astr. Soc.* **253,** 341–349 (1991).
16. Bakowies, D. & Thiel, W. *J. Am. chem. Soc.* **113,** 3704–3714 (1991).
17. Yi, J.-Y. & Bernholc, J. *J. chem. Phys.* **96,** 8634–8636 (1992).
18. Hare, J. P. & Kroto, H. W. *Accts. Chem. Res.* **25,** 106–112 (1992).
19. Kroto, H. W. & Jura, M. *Astr. Astrophys.* **263,** 275–280 (1992).
20. Javahery, G., Petrie, S., Wang, J. & Bohme, D. K. *Chem. Phys. Lett.* **195,** 7–10 (1992).
21. Petrie, S., Javahery, G. & Bohme, D. K. *Astr. Astrophys.* **271,** 662–674 (1993).
22. Millar, T. J. *Mon. Not. R. astr. Soc.* **259,** 35P–39P (1992).
23. von Helden, G., Gotts, N. G. & Bowers, M. T. *Nature* **363,** 60–63 (1993).
24. Su, T. & Bowers, M. T. *Int. J. Mass Spectrom. Ion Phys.* **12,** 347–356 (1973).
25. Javahery, G., Petrie, S., Wincel, H., Wang, J. & Bohme, D. K. *J. Am. chem. Soc.* **115,** 5716–5722 (1993).

ACKNOWLEDGEMENTS. D.K.B. thanks the Natural Sciences and Engineering Research Council of Canada for the financial support of this research, and the Canada Council for a Killam Research Fellowship.

Evidence for strong acidity of the molecular sieve cloverite

Tery L. Barr*, Jacek Klinowski*†, Heyong He*, Klaus Alberti*, Georg Müller‡ & Johannes A. Lercher‡

* Department of Chemistry, University of Cambridge, Lensfield Road, Cambridge CB2 1EW, UK
‡ Institut für physikalische Chemie and Christian Doppler Labor für Heterogene Katalyse, Technische Universität Wien, Getreidemarkt 9/156, A-1060 Wien, Austria

ZEOLITES derive their catalytic activity from the strong acidity of protons attached to the negatively charged aluminosilicate framework, which makes the materials excellent proton donors. Unlike zeolites, the aluminophosphate molecular sieves[1,2] are built from alternating AlO_4^- and PO_4^+ tetrahedra and are thus electrically neutral. Much attention has therefore been devoted to the generation of Brønsted acidity in these materials by introducing heteroatoms, such as Si, Mg, Fe, Co or Zn, to produce negatively charged frameworks[3–6]. Similar arguments apply to gallophosphate molecular sieves[7–10], of which cloverite[9,10] is a remarkable example. This extra-large-pore material contains pore openings in the form of a four-leafed clover, defined by a ring of 20 gallium and phosphorus atoms, some of which are linked to terminal hydroxyl groups. Here we use NMR, X-ray photoelectron spectroscopy (ESCA) and infrared spectroscopy to show that the P–OH groups in cloverite are localized versions of those in solid phosphoric acid, H_3PO_4. Cloverite is thus a strong Brønsted acid even though no heteroatoms are present in its framework.

Cloverite has a cubic structure, $a = 51.712$ Å, with the unit-cell formula $[Ga_{768}P_{768}O_{2,976}(OH)_{192}]\cdot 192QF$, where QF is quinuclidinium fluoride. Single-crystal structural determination[9] shows that there are five crystallographic framework sites for both P and Ga. Pure, highly crystalline cloverite was prepared by the method of Estermann *et al.*[9]. The surface/near surface composition was determined by ESCA to a depth of ~50 Å. The Ga($3p_{3/2}$)/P($2p$) intensity ratio (Fig. 1*a*) gives Ga/P = 1.15, indicating a slight excess of surface gallium, which is consistent with results from related molecular sieves[11]. High-resolution ESCA spectra reveal detailed core-level peak structures for each element. The binding energies and linewidths are given in Table 1, along with those for related materials. The 2.7-eV linewidth of the Ga($3d$) ESCA spectrum (Fig. 1*b* and Table 1) is typical of a distinct gallium species, $GaPO_4$, in the cloverite framework.

The broad and asymmetric P($2p$) ESCA line in Fig. 1*c* signifies the presence of two different oxidic phosphorus-containing species. Deconvolution (Fig. 1*d*) shows that the binding energy of the more abundant P species is 134.1 eV and that of the less abundant species is ~132.3 eV. Although the progressive creation of electron holes in the sample during an ESCA experiment affects the apparent value of the binding energies, a general argument[12–15] allows us to draw conclusions about the initial chemical state from the measured binding energies of oxides. Thus one may assume that, during the formation of an oxide, the more electropositive the element the more negative the O($1s$) binding energy in its oxide. Further, it is known[14,15] that formation of a mixed $A_xM_yO_z$ oxide from two or more simple A_mO_n and M_sO_z oxides will in most cases result in the enhanced covalency of the more covalent of the two metal–oxygen bonds and, conversely, the enhanced ionicity of the more ionic of the two. This manifests itself as a lowering of the binding energy of the more covalently bonded element, and an increase in binding energy of the more ionically bonded. The O($1s$) binding energy for the mixed oxide lies between that of the two simple oxides.

The more intense P($2p$) line represents ~84% of the total phosphorus. This means that the more abundant oxidation state of phosphorus must belong to the Ga–O–P unit in the cloverite framework. The binding energies give a clue as to the nature of the other phosphorus species (~16%). Because of the presence of 'terminal hydroxyl groups' pointing towards the centre of the 20-membered ring, Ga–O–H and P–O–H bonds are present as well as Ga–O–P bonds. The ESCA technique is very sensitive to the nature of M O–H bonds, and the chemical shifts easily distinguish hydroxides from the M–O–M* bonds of the equivalent oxide[14,17]. The M–O–H bonds in cloverite should therefore produce an easily distinguished set of peaks in the appropriate M spectrum. This type of shifted spectral feature is found in the P($2p$) spectrum in Fig. 1*c*, corresponding to P–O–H bonds.

Solid-state NMR and infrared spectroscopy support the above interpretation. The ^{31}P magic-angle-spinning (MAS) NMR spectrum shown in Fig. 2*a* reveals features not seen by Merrouche *et al.*[10] It consists of a main peak at −11.2 p.p.m. with a shoulder at ~−12.6 p.p.m., and a separate smaller line at −6.3 p.p.m. As the intensity ratio of the two lines is 6.84:1, the main peak must correspond to $P(OGa)_4$ structural units, and that at −6.3 p.p.m. to P–OH phosphorus atoms. This ratio is very close to the 7:1 required by the structural determination[9]. The lower ratio of 5.25:1 detected by ESCA (corresponding to a larger population of P–OH groups) is due to the higher surface sensitivity of the technique[12]. The fine structure of the main NMR peak is caused by the presence of four different phosphorus sites. The correct-

TABLE 1 ESCA binding energies and linewidths of cloverite and related materials

	Ga($3d$) (eV)	P($2p$) (eV)	O($1s$) (eV)	Al($2p$) (eV)	Reference
P–O–Ga in cloverite	21.6 (2.7)	134.1 (2.3) [0.84]	531.9 (2.5)	–	This letter
P–O–H in cloverite	–	132.3 (2.3) [0.16]	531.9 (2.5)	–	This letter
$AlPO_4$-8	–	135.0 (2.4)	532.8 (2.2)	75.4 (2.4)	23
Na_2HPO_4	–	133.1	NA	–	16
Na_3PO_4	–	132.3	NA	–	16
Ga_2O_3	20.5	–	530.9	–	16
P_2O_5	–	135.2	533	–	16
Al_2O_3	–	–	531.0 (2.0)	74.0 (2.1)	12, 16

Selected binding energies and (in round brackets) linewidths ± 0.2 eV, referenced to C($1s$) = 284.6 eV from the quinuclidinium $-CH_2$ groups. The justification for this method of removing charging shifts has been given previously[12,16,22]. Relative intensities are given in square brackets. The total linewidth of the overlapping P($2p$) lines from P–O–Ga and P–O–H in cloverite is 3.0 eV. NA, not applicable.

† To whom correspondence should be addressed.